

Supplementary Information

submitted to *Materials Advances*

Tunable and Ordered Porous Carbons with Folding-Like Nanoscale Framework *via* Interdigitation and Twisting

Shiori Kubo*

National Institute of Advanced Industrial Science and Technology (AIST),
1-1-1, Higashi, Tsukuba, 305-8561, Japan

Details of material characterization

X-ray diffraction patterns were recorded on a Rigaku SmartLab (Rigaku Corp.) with Cu K α equipped with a D/teX Ultra 2250 detector at a voltage of 40 kV and current of 45 mA. For the analyses of pore properties of the materials from the results of the nitrogen gas sorption measurement, Brunauer–Emmett–Teller (BET) calculations were performed for obtaining the surface areas (S_{BET}). Total pore volume was calculated from the adsorbed volume at $P/P_0=0.99$ of adsorption curve using the equation: $V_{total} = V_{ads}^{N_2@STP}[\text{cm}^3 \text{g}^{-1}] \times 10^{-3} / 22.4$ [L mol $^{-1}$, (the ideal gas constant)] $\times 28$ [g mol $^{-1}$, (molecular weight of the nitrogen molecule)] / 0.808 [g cm $^{-3}$, (density of liquid nitrogen)]. Pore size distribution and V_{micro} value were calculated using the NLDFT method of the BELMasterTM software (BEL JAPAN, Inc), based on the adsorption branch of the isotherms and on the carbon slit pore model. The sum of pore volume (cumulative pore volume) deriving from the pores smaller than 2 nm was taken as V_{micro} . Mesopore volume (V_{meso}) was calculated by subtracting V_{total} from V_{micro} . In the transmission electron micrographs presented, Fig. 4A is a combined image of two micrographs with the observation fields next to each other and captured separately (due to the size limitation of the capture area of the detector. The joint is marked by a dotted line). Image contrast is increased for enhanced image clarity for Fig. 4E using a Gatan Microscopy Suite® software.

Supplementary Figures

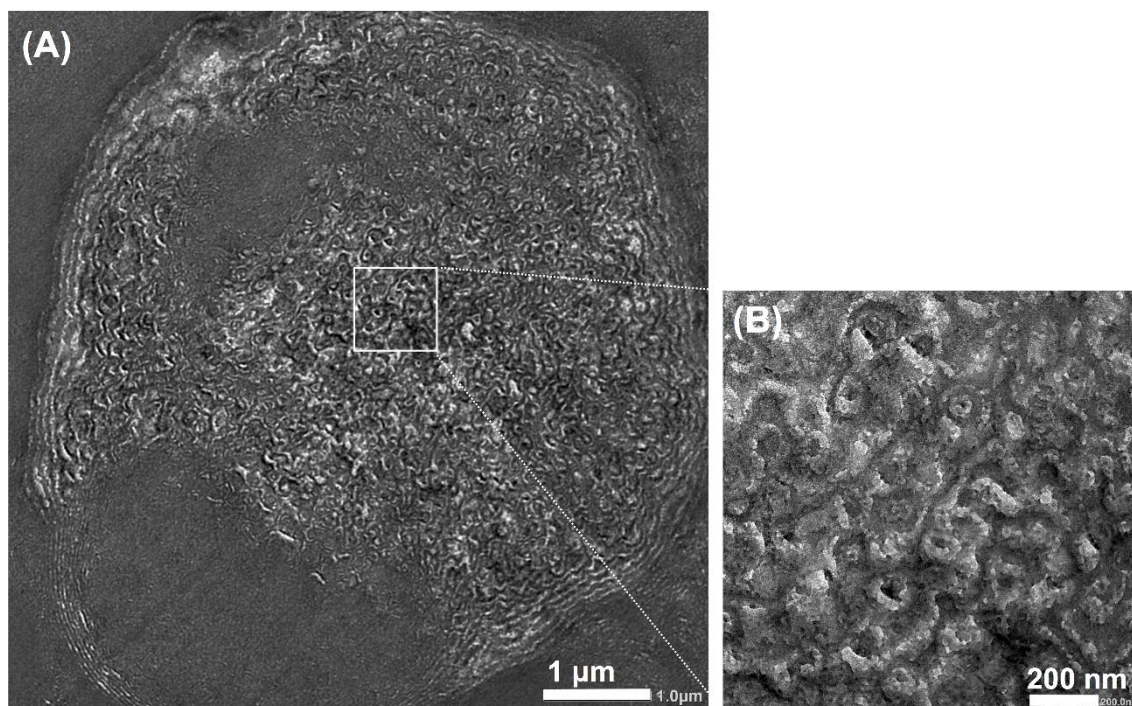


Figure S1. (A-B) Mixed lamellae-like and gyroidal nanostructure of the composite of template polymer and carbonaceous moieties (synthesized from D-fructose precursor). (B) corresponds to high-magnification micrograph of the area highlighted by square in (A).

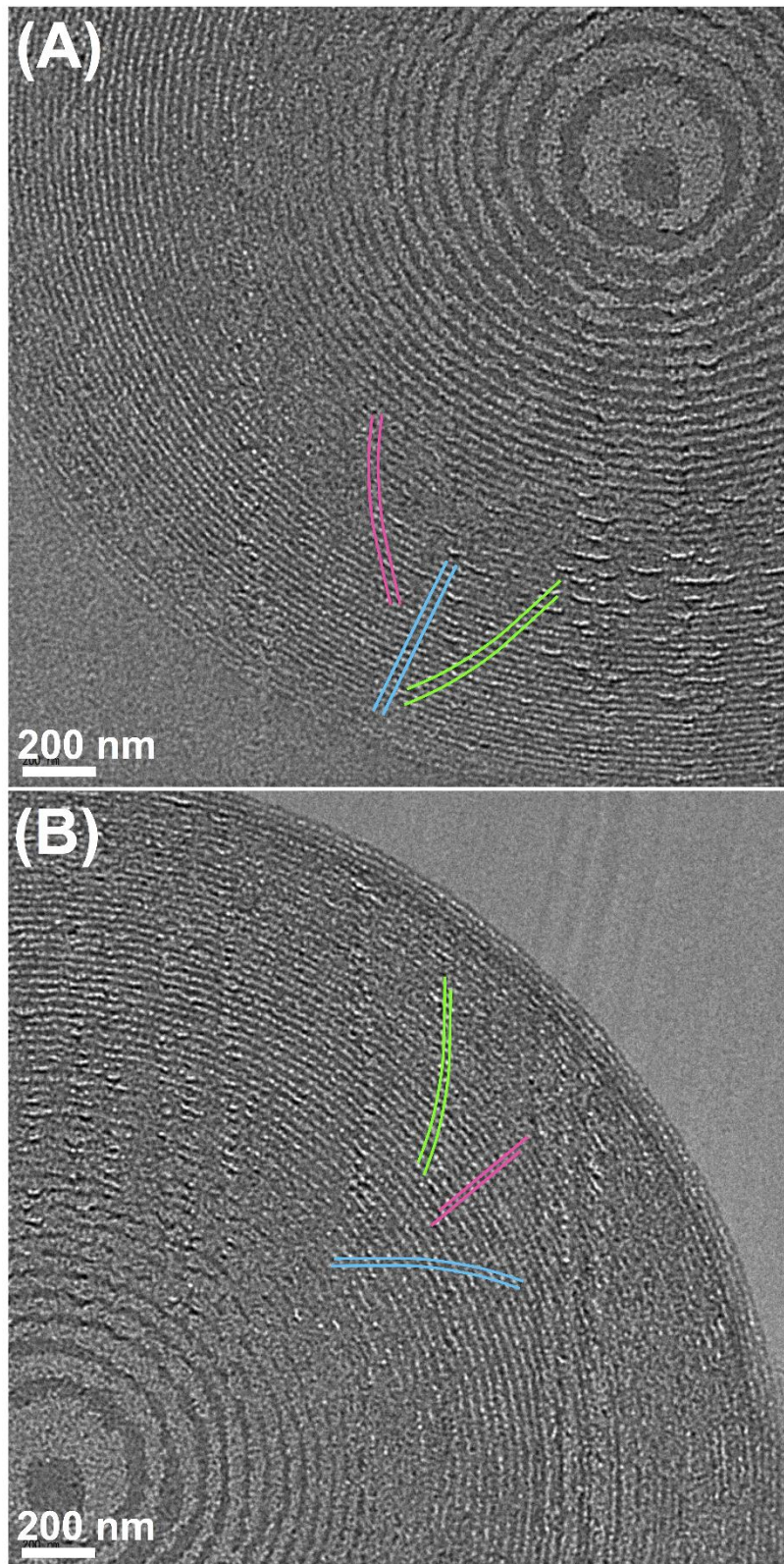


Figure S2. (A) TEM micrographs of the (A) left-down and (B) upper-right areas of the concentric pattern examined in Fig. 4D. Auxiliary conductors for the three layering modes are added for the aiding purpose.

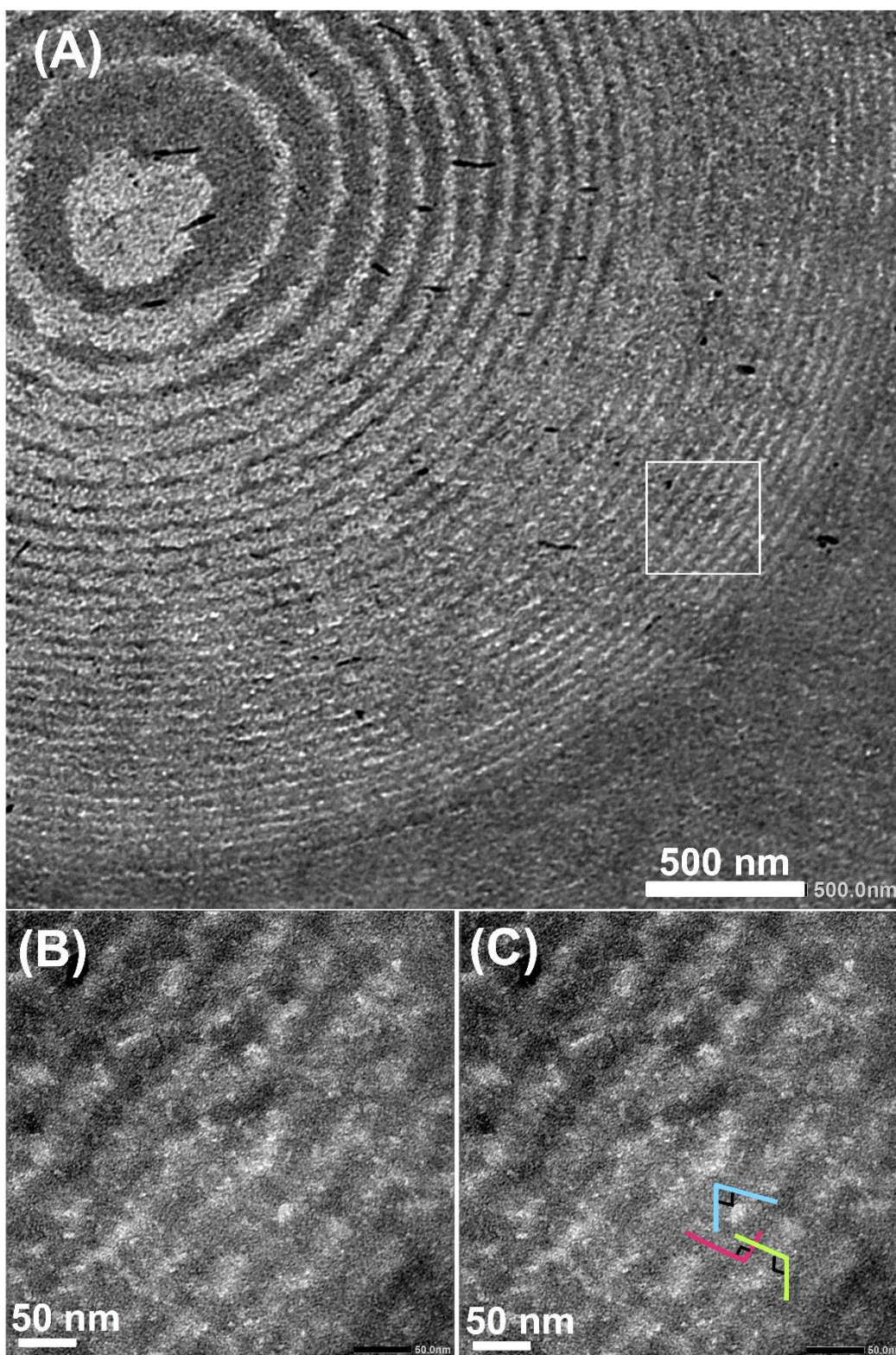


Figure S3. (A) TEM micrographs of the composite of template polymer and carbonaceous moieties showing the concentric pattern. (B-C) High-magnification images of the area highlighted by square in (A). (B) and (C) are identical micrographs, where the auxiliary conductors are added in (C).

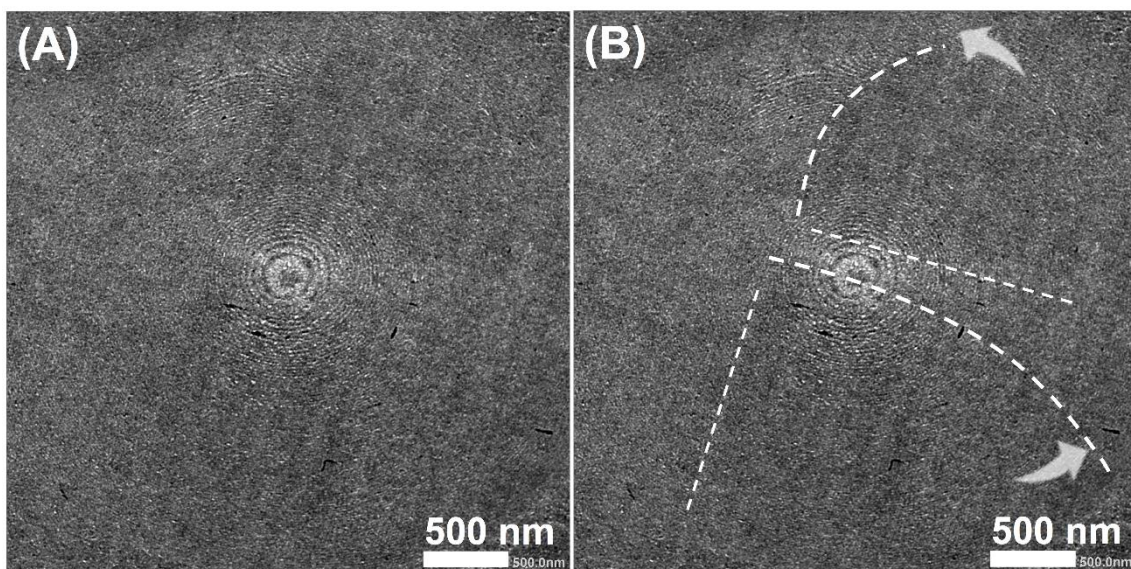


Figure S4. (A) and (B) TEM micrographs of the sliced specimen of the carbonaceous microparticles showing blade-like contrast motifs. (A) and (B) are identical micrographs, where the auxiliary conductors are added in (B).

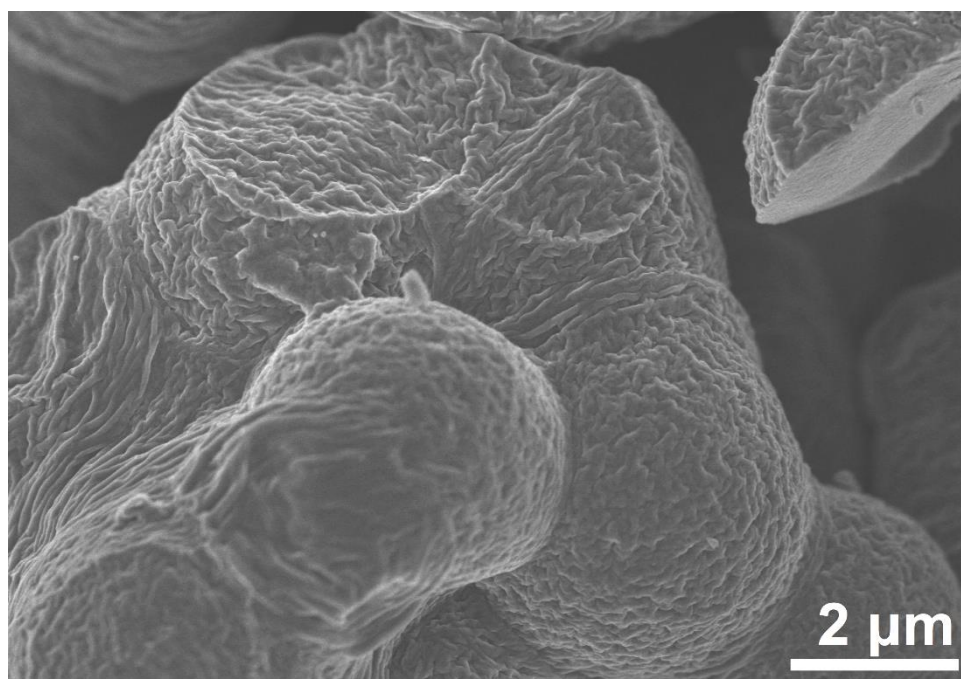


Figure S5. High-magnification SEM micrograph of the resulting microparticles after removal of the polymeric template.

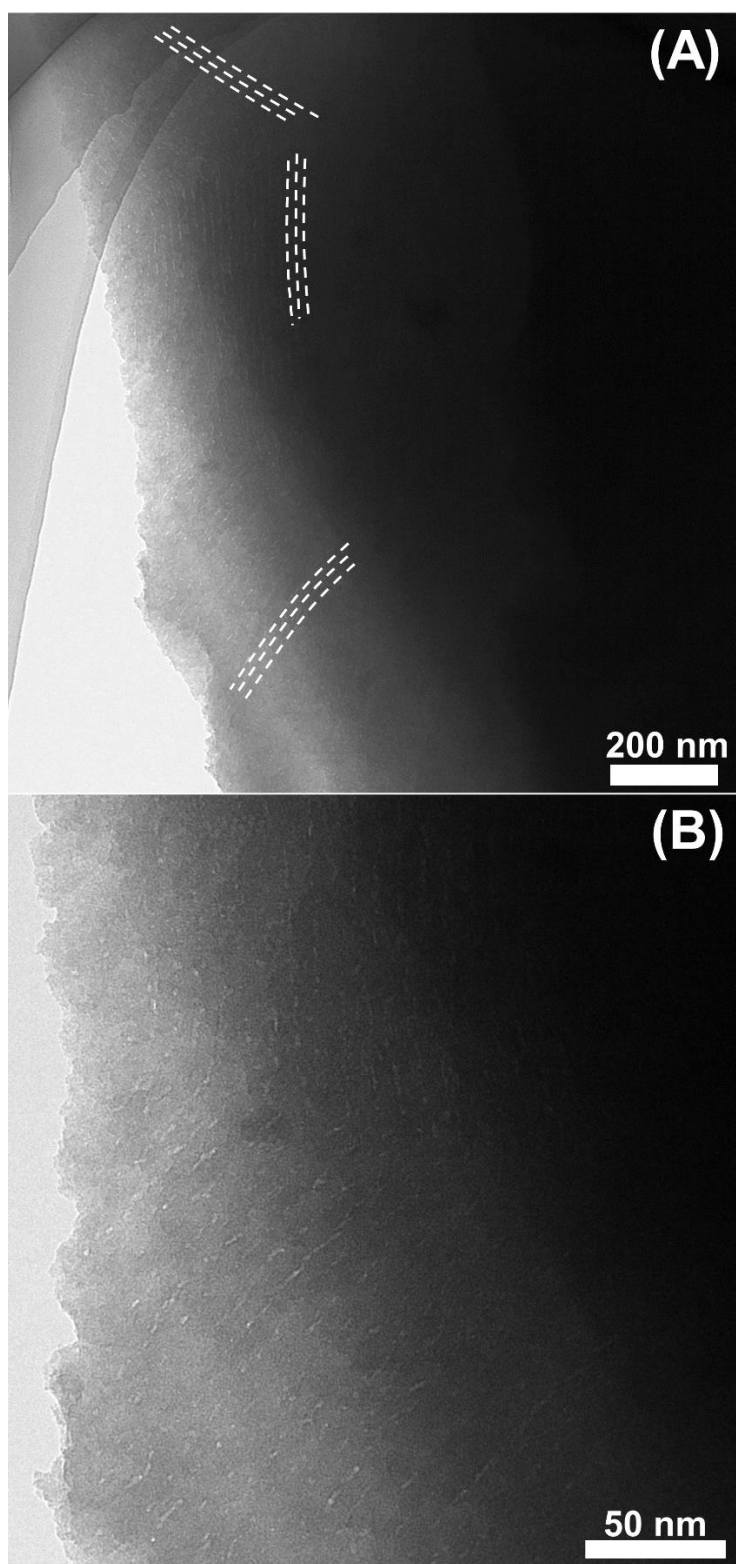


Figure S6. (A) TEM micrograph of the carbonaceous particle resulting after the template removal, showing the lamellae-like textures. The auxiliary conductors are added for indicating the layering modes. (B) Higher-magnification image of (A).

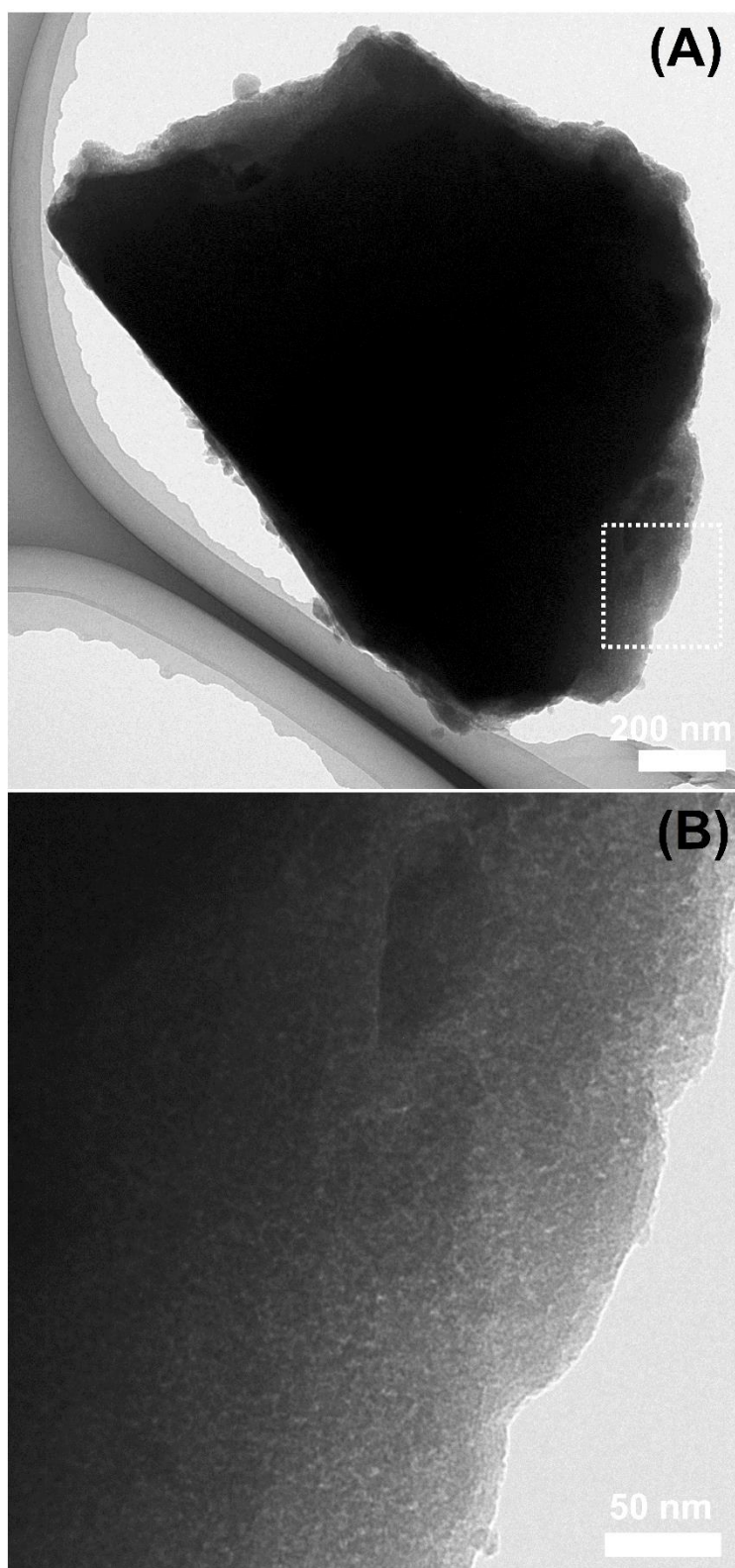


Figure S7. (A-B) TEM micrographs of the carbonaceous particle resulting after the template removal, showing the co-existing gyroidal-like nanoscale textures. (B) corresponds to high-magnification micrograph of the area highlighted by square in (A).

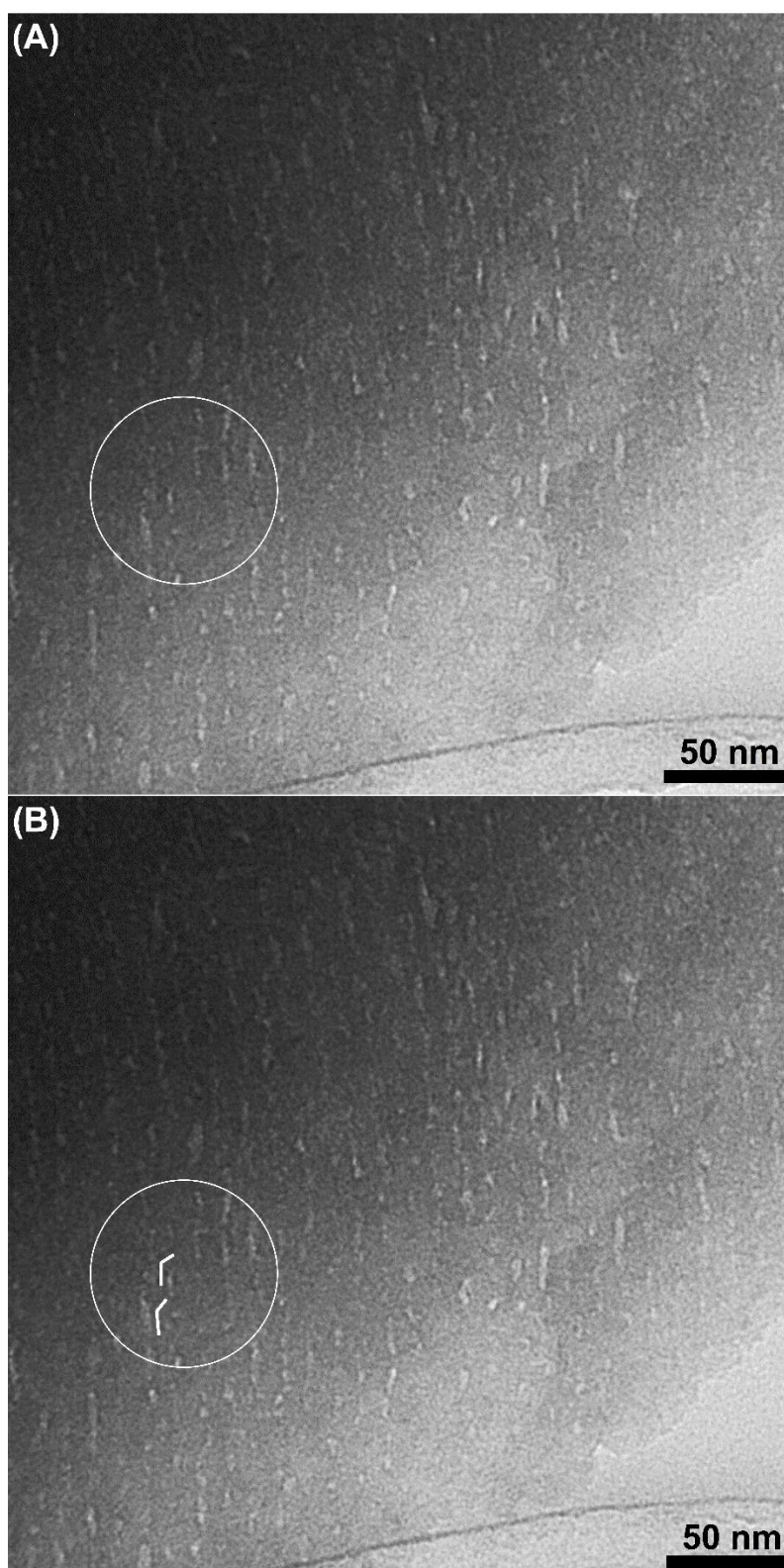


Figure S8. (A-B) Higher-magnification TEM images of the area indicated by the arrow in Fig. 5C. (A) and (B) are identical micrographs, where a local knotting-like texture in the area highlighted by circle is indicated by white lines in (B).

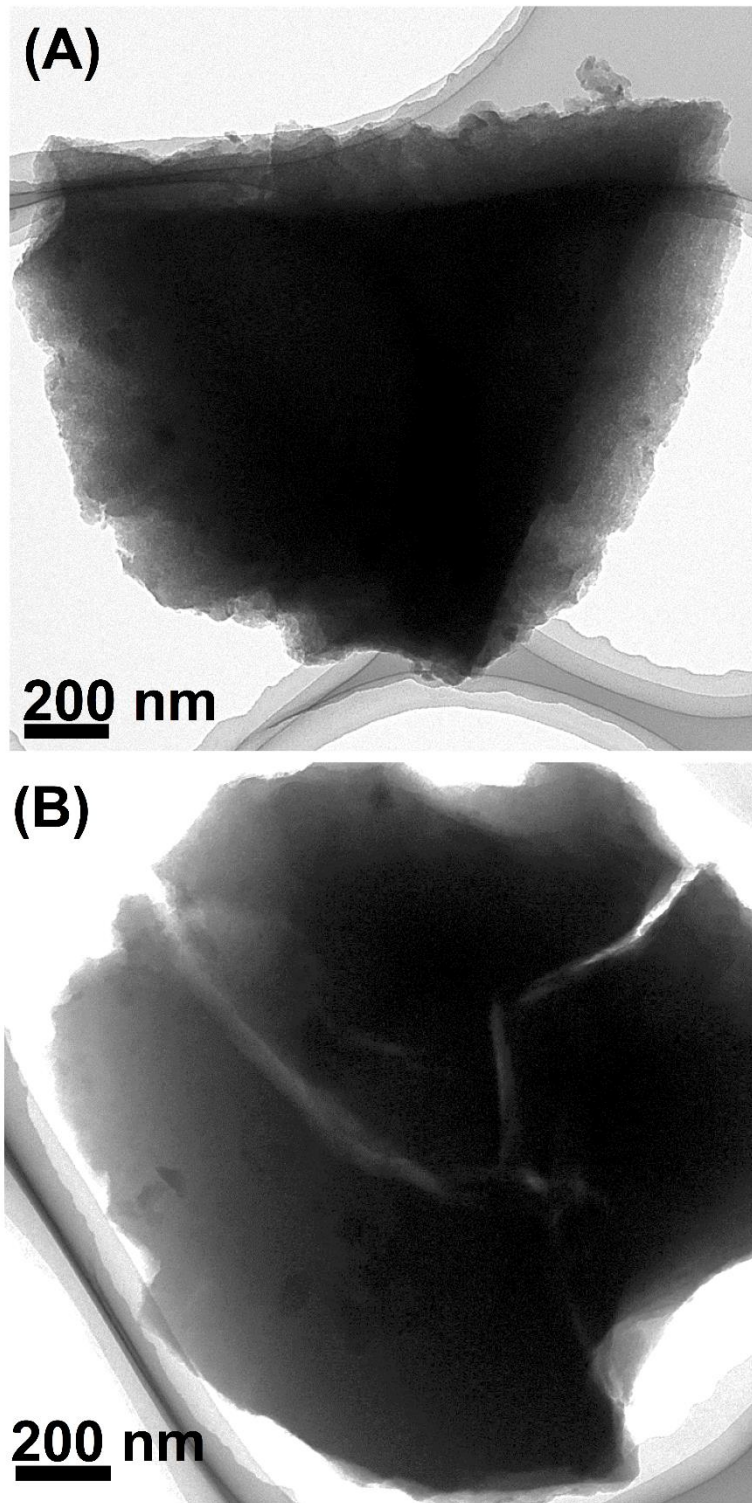


Figure S9. (A) and (B) TEM micrographs of the ground carbonaceous particles (after template removal *via* calcination) showing the three cleavage directions.

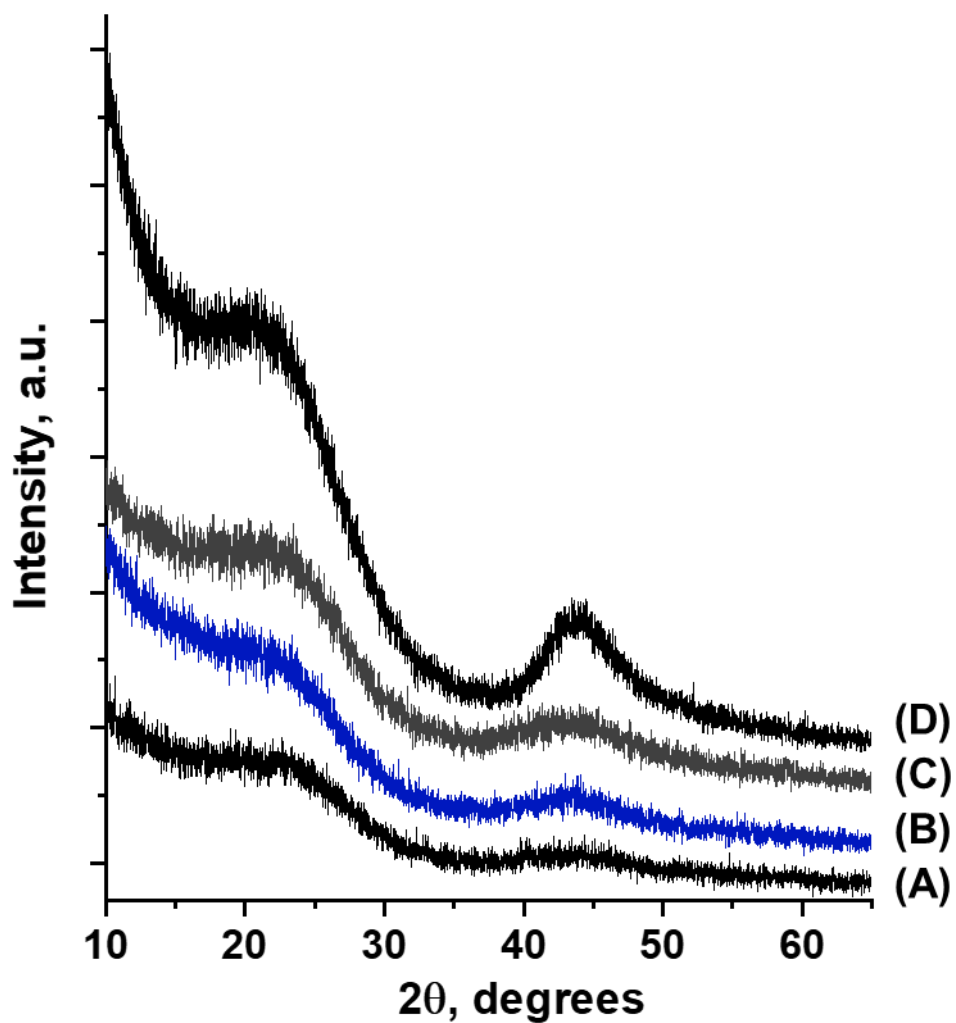


Figure. S10. X-ray diffraction patterns of the carbonaceous materials with the folded nanoscale framework (after template removal) synthesized (A) with D-fructose, (B) with L-fructose, (C) with D-fructose in a concentrated system, and (D) with D-fructose in a concentrated system and calcined at 900 °C.

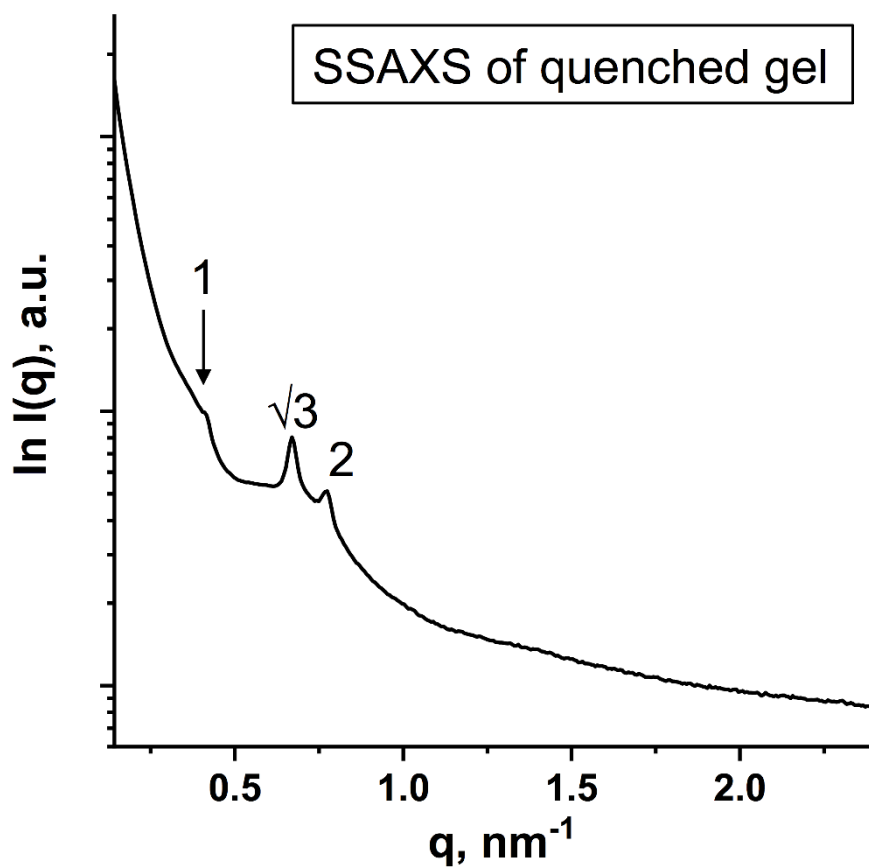


Figure S11. Synchrotron SAXS pattern of the quenched gel-like material obtained within 24h of hydrothermal treatment of the starting solution.

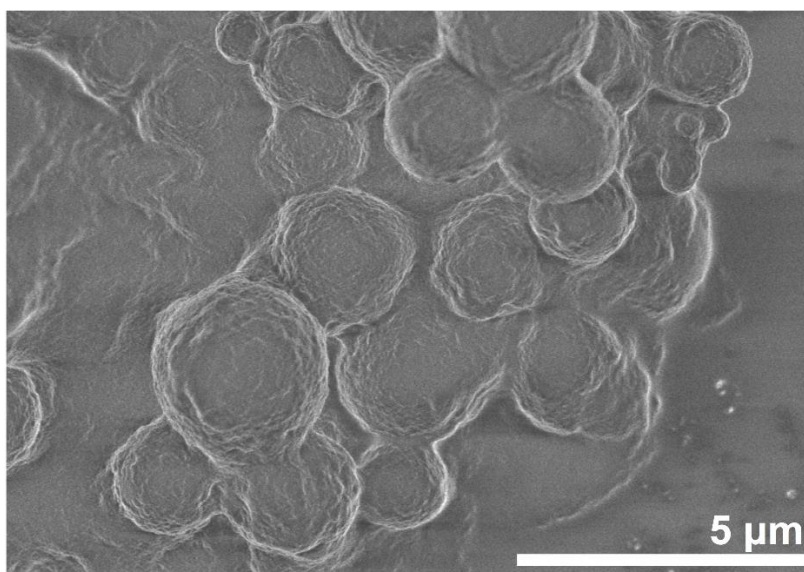


Figure S12. SEM micrograph of the composite of template polymer and carbonaceous moieties derived from the synthesis using L-fructose precursor.

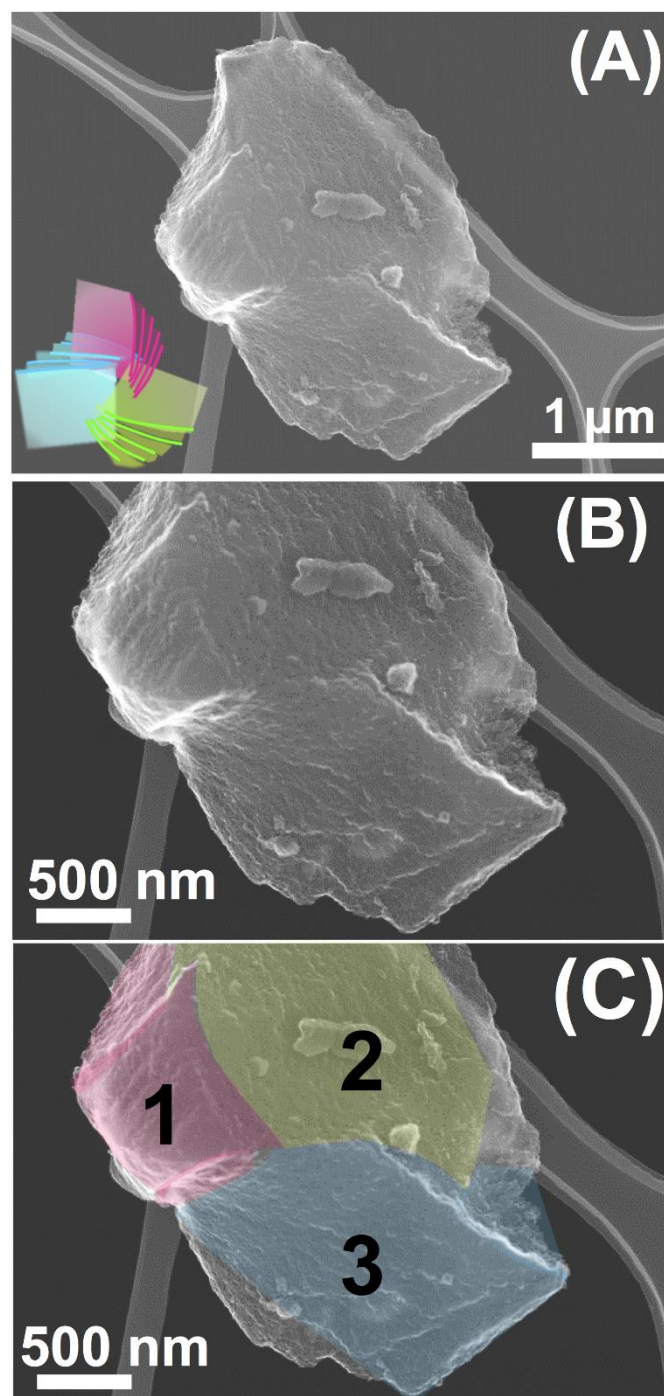


Figure S13. (A)-(C) SEM micrographs of cleaved specimen of calcined L-Fru-derived carbonaceous particle showing interpenetration of three individual modules (inset) the structural model shown in Fig. 3A, with right-handed configuration. (B) and (C) are identical micrographs, while the auxiliary colors indicating three layered modules are added in (C).

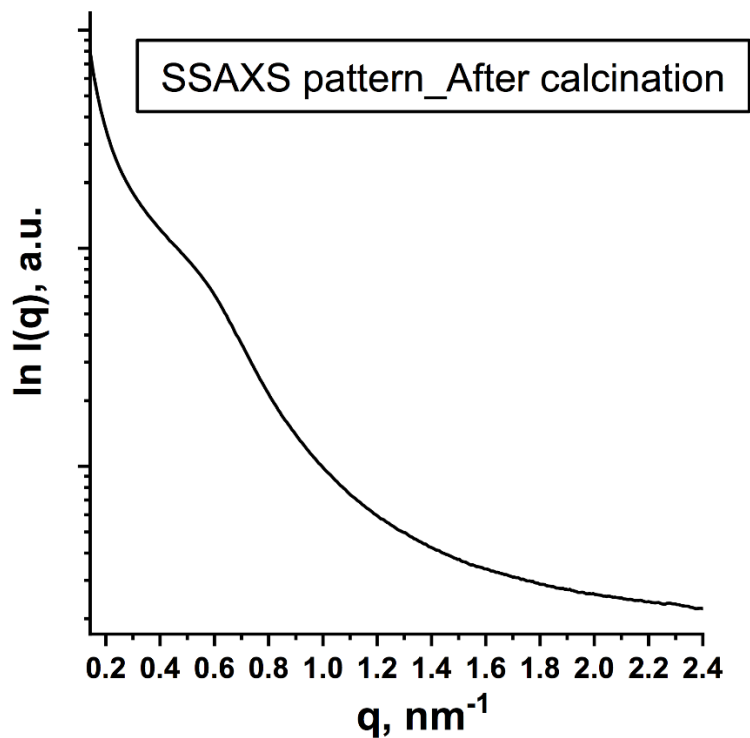


Figure S14. SSAXS pattern of the L-fructose-derived carbonaceous materials after calcination.

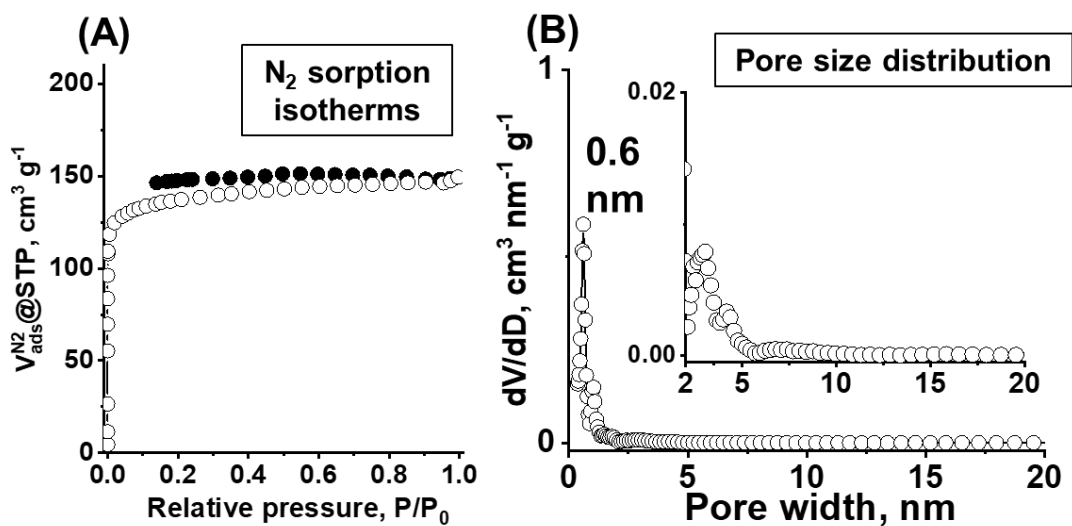


Figure S15. (A) Nitrogen sorption isotherms and (B) DFT pore size distribution curve of L-fructose-derived porous carbonaceous material.

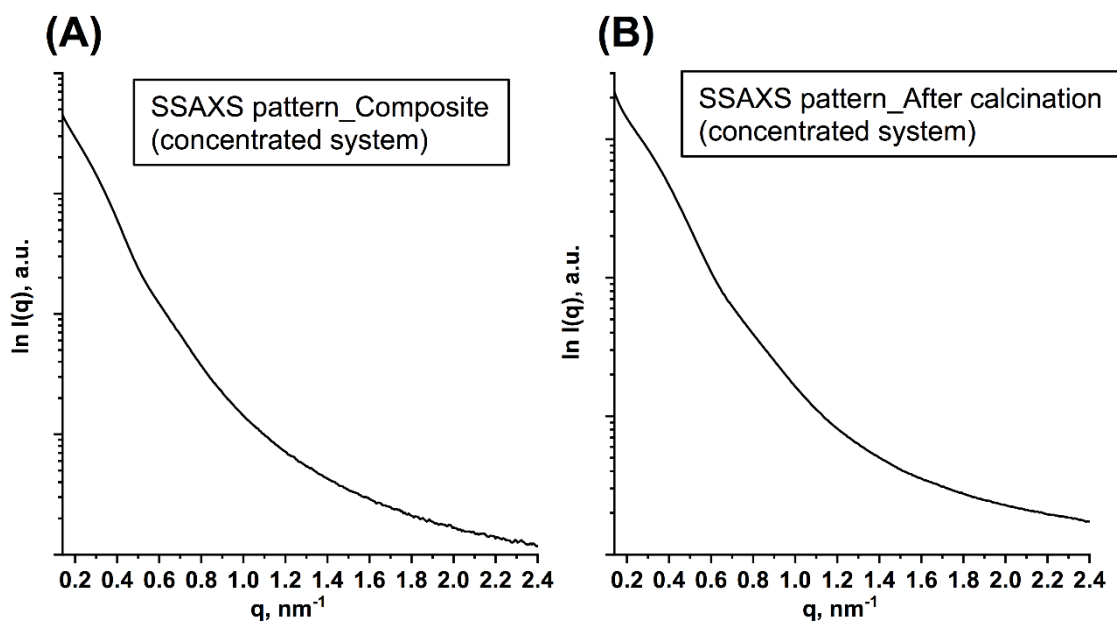


Figure S16. SSAXS patterns of the materials synthesized at a higher polymer concentration (for pore expansion): (A) before and (B) after template removal.

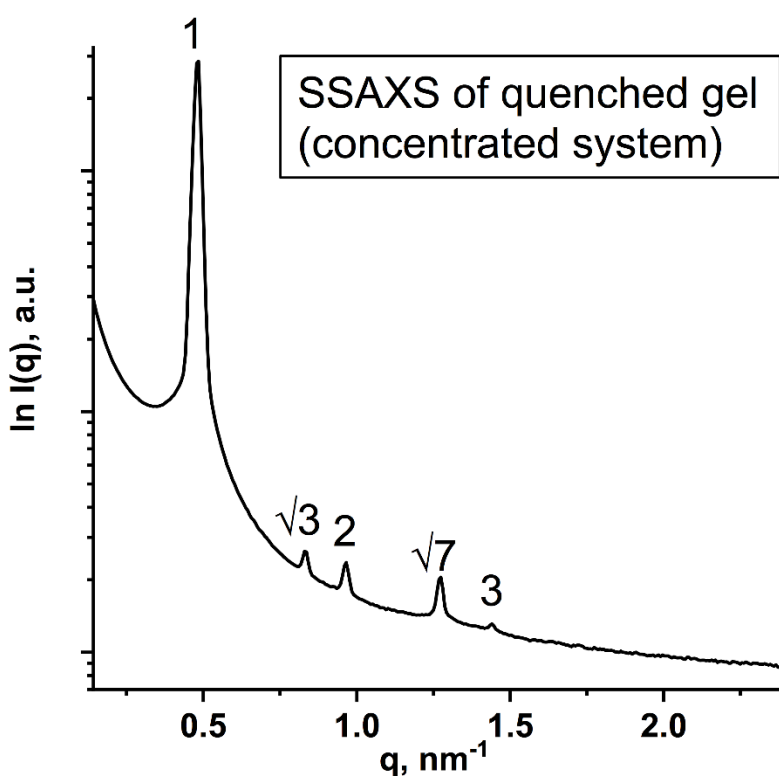


Figure S17. SSAXS pattern of the quenched gel obtained within 24h of hydrothermal treatment of the starting solution in the concentrated system.

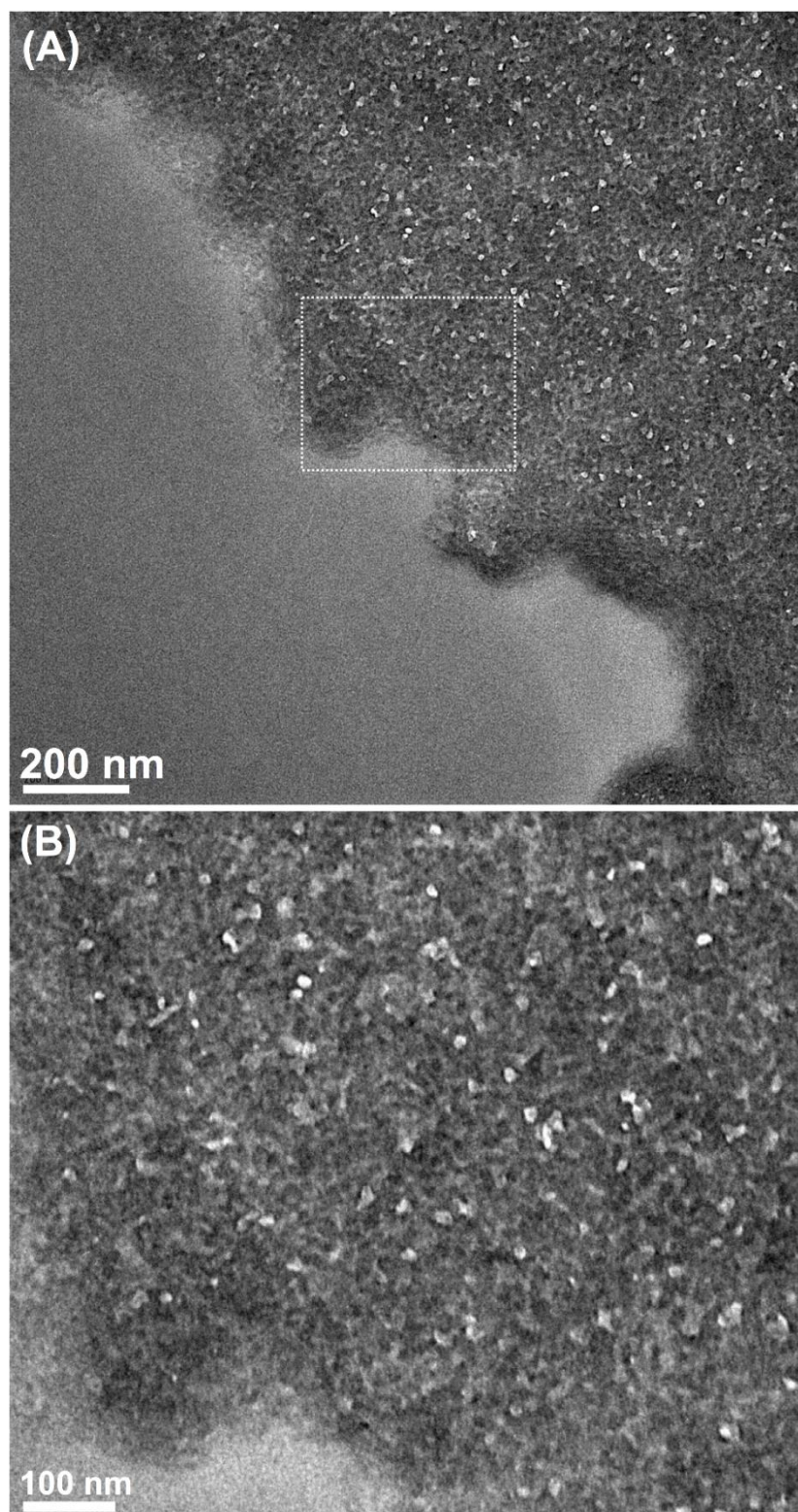


Figure S18. (A) TEM micrograph of the as-synthesized composite of polymer template and carbonaceous moieties prepared at a higher template concentration. (B) High-magnification micrograph of the area highlighted by square in (A).

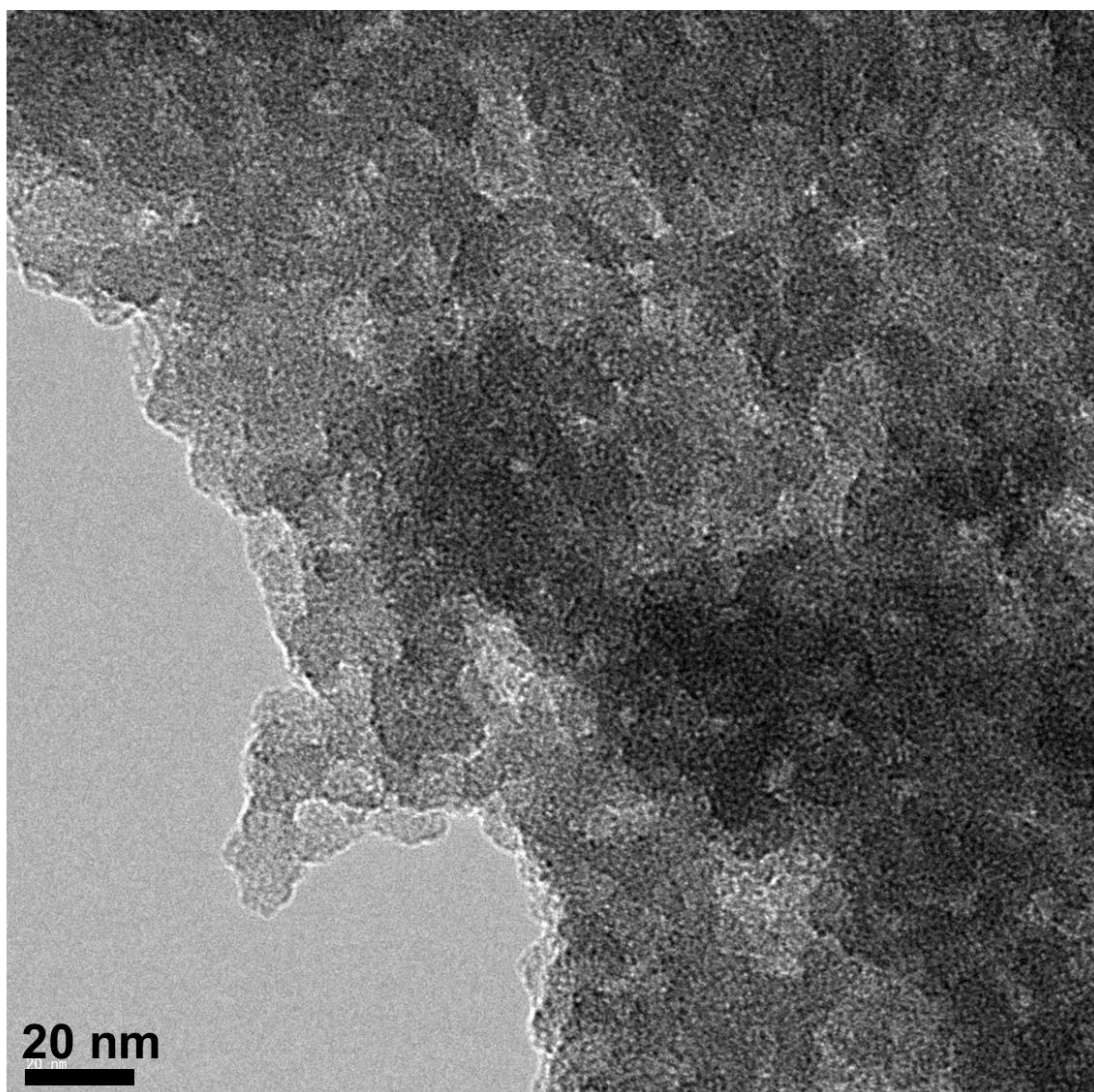


Figure S19. TEM micrograph of the as-synthesized composite of polymer template and carbonaceous moieties prepared at a higher polymer concentration taken at a higher magnification (non-ultramicrotome specimen).

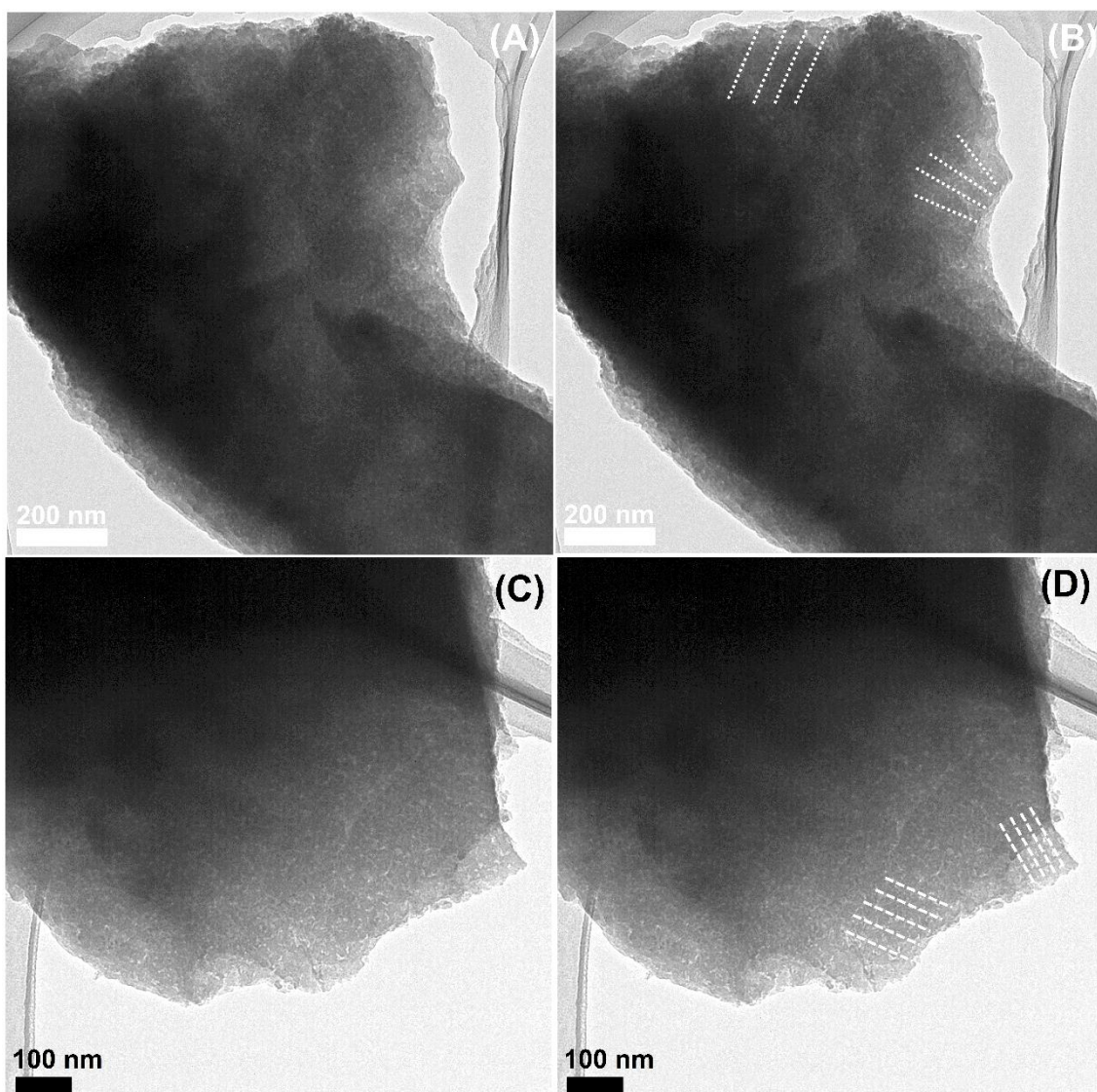


Figure S20. TEM micrographs of the carbonaceous materials prepared at a higher polymer concentration for pore expansion. (A) and (B), and (C) and (D) are identical micrographs, respectively, where lines in (B) and (D) indicate developing directions of the nanoscale layering modes.

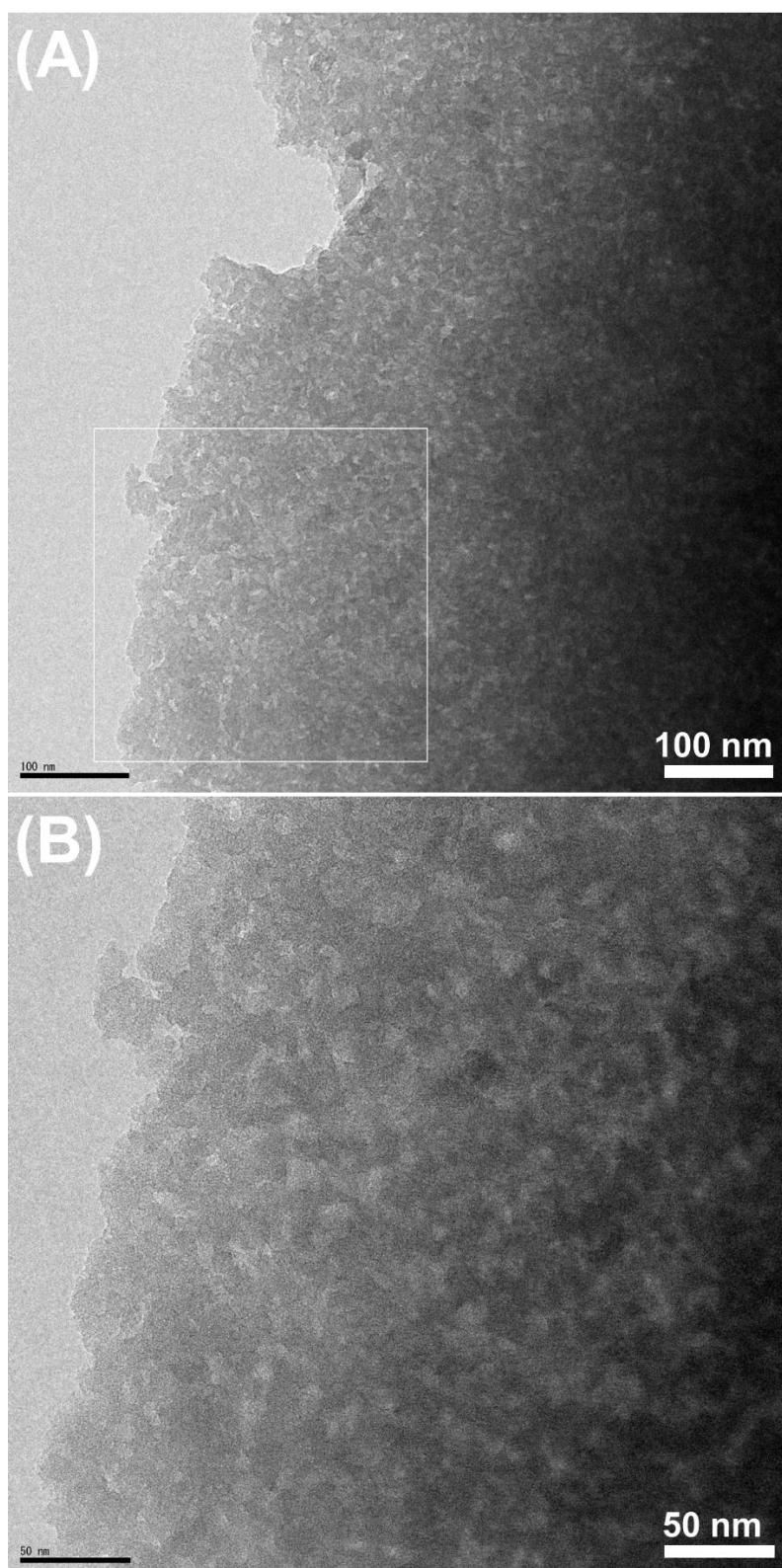


Figure S21 (A) (B) High-magnification TEM micrographs of the carbonaceous materials prepared at a higher polymer concentration. (B) corresponds to the micrograph of the area highlighted by square in (A), taken at a higher magnification.

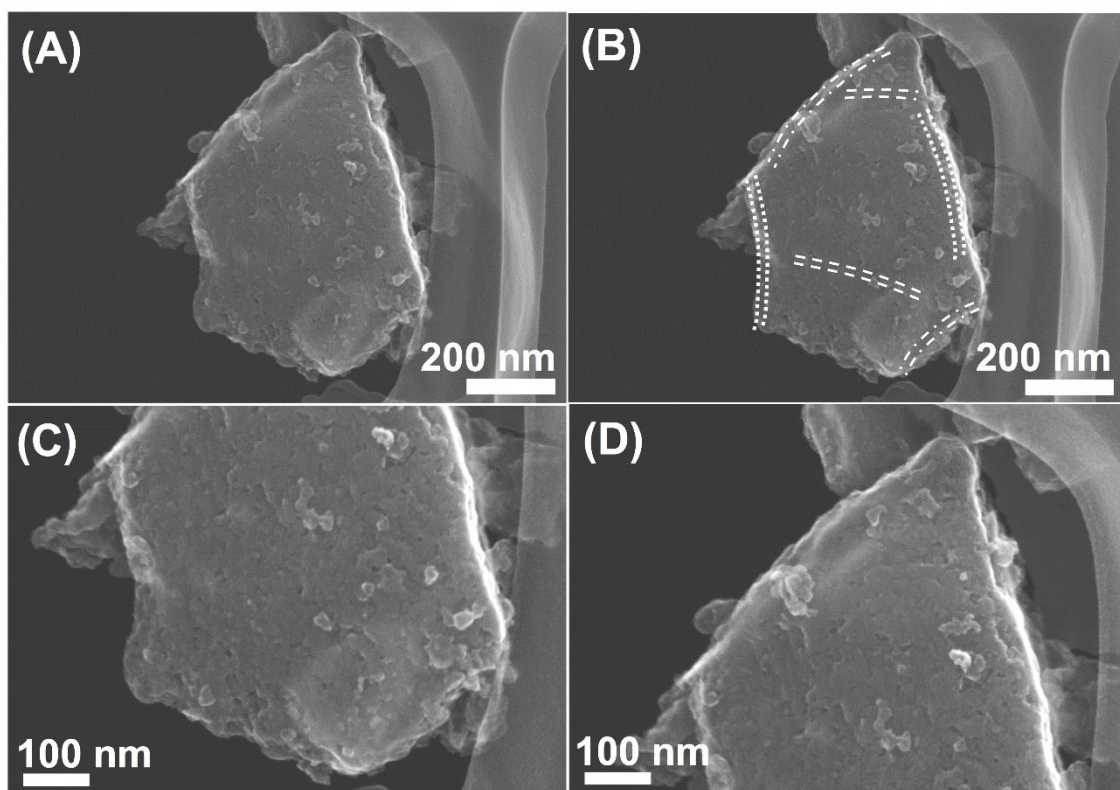


Figure S22. SEM images of the carbonaceous particles after mechanical grinding, synthesized under a concentrated template system. (A) and (B) are identical micrographs, where the auxiliary lines are added in (B) to indicate the development of three lamellae-like phases. (C) and (D) are high-magnification micrographs of the particle shown in (A-B).

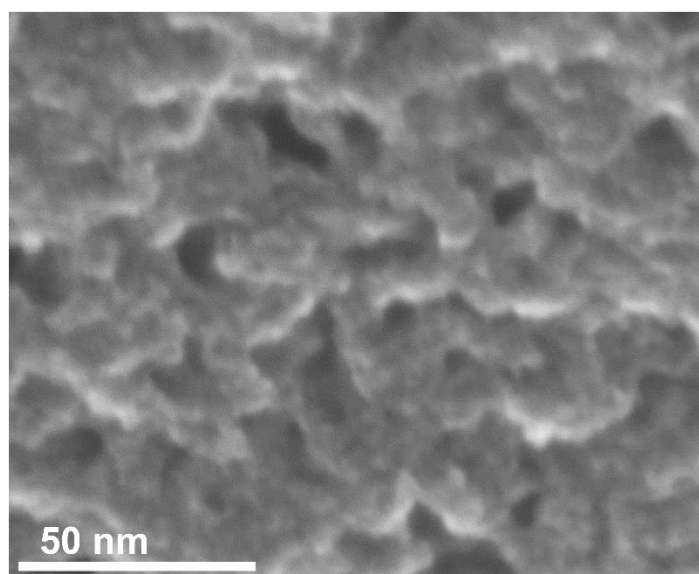


Figure S23. High-magnification SEM image of the carbonaceous nanostructure formed by synthesis at a higher polymer concentration (after template removal *via* calcination).